Thesis

A Study of the Feasibility of Detecting Primordial Microscopic Black Hole Remnants with the NOvA Far Detector

Submitted by

Megan Wrobel

Department of Physics

In partial fulfillment of the requirements

For the Degree of Master of Science

Colorado State University

Fort Collins, Colorado

Spring 2024

Master's Committee:

Advisor: Norm Buchanan

Josh Berger
Henry Adams

Abstract

A Study of the Feasibility of Detecting Primordial Microscopic Black Hole Remnants with the NOvA Far Detector

Several papers have argued that microscopic black holes may be stable against complete evaporation and may be a viable dark matter candidate [1–3]. This paper assesses the practicality of detecting these objects using long-baseline neutrino facilities, such as the NuMI Off-Axis ν_e Appearance (NOvA) experiment and the Deep Underground Neutrino Experiment (DUNE). The origin, stability, properties, and energy loss mechanism of such objects are examined. The signals produced from the detectors should allow for discrimination between these microscopic black holes and other particles traversing the detector. Potential challenges that could arise and next steps are also identified and considered.

Acknowledgements

I would like to express my sincere gratitude to my thesis advisor, Norm Buchanan, for his unwavering support and invaluable guidance throughout this research journey. I am also deeply thankful to my committee members, Josh Berger and Henry Adams, for their constructive feedback and thoughtful insight. Finally, I would like to thank Jackson Benz for the important contributions he provided to this project.

Thank you all for your collective insights and support.

Table of Contents

List of Tables

List of Figures

CHAPTER 1

Introduction

Throughout the last few decades, there has been great interest in black holes (BHs) as potential dark matter candidates [4–6]. The observable universe is generally thought to comprise about 72% dark energy, 24% dark matter, and only 4% ordinary matter. Gravity is the only force that we know for certain interacts with dark matter, and the simplest assumption is that gravity is the only force coupled to dark matter; no strong argument exists that the weak interaction should necessarily be taken into account in dark matter interactions [3].

In 1974 and 1975, Stephen Hawking published his analysis of the effects of gravitational collapse on quantum fields and predicted that BHs give off thermal radiation and eventually explode [7, 8]. A key challenge is showing that BHs cease to radiate under certain conditions, which could then be used as an argument to explain how these objects can survive from the early universe [3]. Hawking also proposed that unidentified tracks in the photographs taken in bubble chamber detectors could be explained as signals of gravitationally collapsed objects; we will refer to such objects as microscopic black hole (BH) remnants.

This thesis will summarize the origin and stability of microscopic BHs by assuming that there is a mechanism by which evaporation can be halted at the Planck scale, allowing these objects to exist. Furthermore, this thesis will provide an assessment the feasibility of direct detection of these objects and how their signals may be distinguishable from other particles. The challenges and next steps of this analysis will also be presented.

CHAPTER 2

Motivation and Theory

2.1. Formation

The process of BH formation is well known [9]. Due to density fluctuations in the early universe, numerous gravitationally collapsed objects can be formed with characteristics governed by gravity and quantum phenomena; for masses above the Planck mass limit of 10^{-5} g, quantum behavior does not play a role [3]. Hawking suggests that it is likely that BHs could not form with radii of order less than 10^{-33} cm, the Planck length; a Schwarzschild radius of this length would correspond to a mass of about 10^{-5} g, the Planck mass, via the equation

$$R = \frac{2GM}{c^2} \tag{1}$$

where G is the universal gravitational constant, M is the mass of the BH, and c is the speed of light.

In standard BH thermodynamics, there is no direct answer as to whether a small BH such as this would evaporate entirely, via Hawking radiation, or leave behind a BH remnant [1]. A small BH should emit blackbody radiation, becoming lighter and hotter, until it reaches an explosive end when the mass approaches zero; however, Hawking's original calculation relies on classical assumptions. These assumptions must break down as the BH becomes smaller and lighter.

According to Helfer [10], a primordial BH that formed in the early universe, assuming the effects of Hawking radiation, would need to possess a minimum mass on the order of

10^{15} g in order to survive to the present day; this can be seen via the equation

$$t_{life} \sim \left(\frac{M}{M_\odot}\right)^3 \cdot 10^{65} \text{ y} \tag{2}$$

by setting t_{life} to the present age of the universe, and where $M_\odot$ is the mass of the Sun.

Furthermore, any primordial BH produced with a mass below about 5×10^{14} g will evaporate to the Planck scale by the present day; any BH created with a mass less than about 10^{16} g has an initial temperature on the order of 1 MeV ($\sim 10^{10}$ K), consequently emitting charged leptons rapidly enough to acquire a spontaneous charge, though it will continue to evaporate today [11, 12].

2.2. Hawking Radiation, Evaporation, and Stability at the Planck Scale

Hawking argues that in order for a BH to form, its electrostatic energy must be less than its gravitational energy

$$Z^2 e^2 R^{-1} < GM^2 R^{-1} \tag{3}$$

where Z is the charge of the hole, e is the elementary charge, and R is the Schwarzschild radius given by Equation 1.

If we let M be the Planck mass, which is of order

$$M_P \sim \sqrt{\frac{hc}{G}} \tag{4}$$

where h is Planck's constant, then we see that $Z^2 < (hc/e^2)$. Noting that $e^2 \sim (\alpha hc/2\pi)$, then $(hc/e^2) \sim (2\pi/\alpha) \sim 900$, where α is the fine-structure constant. Thus, we expect that BHs can carry an electric charge $|Z|$ of up to 30, in electron units [3, 13].

An imperative issue is showing that, under certain conditions, BHs do not emit radiation. This is essential for understanding how these remnant objects can survive from the early universe, though this issue remains unresolved [3]. Currently, there is no compelling theory explaining non-radiating microscopic BHs. In fact, the prediction that BHs emit radiation due to quantum phenomena is regarded as one of the most secure predictions in quantum field theory [10]. However, this prediction relies on two assumptions: that our current understanding of physics can be applied to vacuum fluctuations at energy scales that are increasing exponentially and are bounded by the Planck scale; and that quantum gravitational effects can be neglected.

Small BHs are thought to be unstable due to Hawking radiation; however, this mechanism is not well understood for masses on the order of the Planck scale [3]. In fact, Helfer argues that none of the derivations provided regarding the prediction of radiation from BHs is convincing [10]. All of the derivations that have been put forward, none of which are mutually consistent, involve speculations on the physics at scales that are not just orders of magnitude beyond any that have been investigated experimentally, but also at the Planck scale; the effects of quantum gravity are expected to be dominant in this regime.

There exist equally plausible speculations regarding the physics at these scales that lead to the absence of any radiation at all [10]. For example, Adler suggests that a small BH should radiate photons and other particles via Hawking radiation until it reaches the Planck scale, at which point radiation halts, and the BH's entropy reaches zero, despite its effective temperature reaching a maximum; thus, the BH cannot emit additional radiation, becoming an inert remnant [1]. As the BH undergoes the process of evaporation, charged particles of both signs are emitted stochastically; thus, during this process, non-zero electric charges are

produced [3, 11]. Should evaporation suddenly cease at some mass scale on the order of the Planck mass, the BH could retain a residual electric charge of a random sign [11].

The generalized uncertainty principle (GUP) has been used to argue that total evaporation may be prevented, and thus, a BH remnant with Planck mass and size would exist [2]. The GUP may prevent complete BH evaporation in the same way that the hydrogen atom is prevented from total collapse by the standard uncertainty principle, prevented not by symmetry, but by dynamics [1].

The GUP gives the BH position uncertainty as

$$\Delta x \geq \frac{\hbar}{\Delta p} + L_P^2 \frac{\Delta p}{\hbar} \tag{5}$$

where Δx and Δp are the position and momentum uncertainties respectively, $\hbar$ is the reduced Planck's constant, and

$$L_P = \sqrt{\frac{G\hbar}{c^3}} \tag{6}$$

is the Planck distance.

We can understand this in the following way. Consider a particle, such as an electron, being observed by means of a photon of momentum p. The familiar Heisenberg argument gives rise to the position uncertainty of the electron, given by the first term in Equation 5. However, if we include a term for the gravitational interaction between the electron and photon, we will have a term proportional to Gpc, or G times the photon energy. The momentum uncertainty of the electron, Δp, will be of order p; thus, on dimensional grounds, this term must be of order $G\Delta p/c^3$, which is equivalent to the second term in Equation 5.

Now, solving Equation 5 for the momentum uncertainty in terms of the distance uncertainty, we find the momentum for radiated photons

$$\frac{\Delta p}{\hbar} = \frac{\Delta x}{2L_P^2}\left[1 \mp \sqrt{1 - 4L_P^2/\Delta x^2}\right] \tag{7}$$

Identifying Δpc as the characteristic energy of an emitted photon, and thus the characteristic temperature, we can also find the temperature for radiated photons

$$T_{GUP} = \frac{Mc^2}{2\pi}\left[1 \mp \sqrt{1 - M_P^2/M^2}\right] \tag{8}$$

We see that the temperature becomes complex and nonphysical for mass less than the Planck mass and Schwarzschild radius of order less than the Planck length, the minimum size allowed by the GUP [1].

2.3. Properties

Each isolated, stationary BH occurring in nature can be characterized by its mass, angular momentum, and charge [10]. A BH with a mass below 10^{14} g today is expected to possess a spin parameter extremely close to zero, so the impact of angular momentum on the BH metric should be negligible and will be considered so for this thesis. [11].

A neutral BH can spontaneously acquire electric charge by emitting a charged particle. On the other hand, as a charged BH emits particles and antiparticles stochastically and accumulates either a positive or negative net charge, it will have a tendency to emit more particles of that same charge polarity, pushing the BH toward a state of neutrality. In either case, the spontaneous charge of a small BH fluctuates rapidly around neutrality [11, 12]. Hawking argues that this process of neutralization would continue until the temperature of

the BH falls to the point where the wavelength of the emitted particles was greater than the radius of the BH [3, 13]. Page [12] conducted a numerical analysis of the distribution of BH charges and found if a BH is sufficiently small to emit charged leptons rapidly, and if this process continues for a long enough duration that many particles are emitted, the fluctuations will result in a certain stationary probability distribution for the BH's charge; this equilibrium charge distribution is approximately Gaussian

$$P(Z) \sim \exp(-4\pi\alpha(Z/e)^2) \tag{9}$$

where α is the fine-structure constant [11, 12].

Lehmann suggests that a small BH cannot retain even one elementary charge for a significant duration, so long as the process of evaporation continues. In the low mass regime, where the timescale for Hawking emission is extremely short, any charge acquired through accretion will likely be nullified by the evaporation processes, and the equilibrium distribution will be maintained. However, it is important to note that the validity of directly extrapolating Page's charge distribution to the Planck scale remains uncertain. Quantum gravity corrections are likely significant at this scale, and it is unknown how this might influence the charge distribution [11]. Lehmann argues that Planck-scale remnants of evaporating primordial BHs may generically have charges on the order of e, and reasonable forms of their mass spectrum result in a substantial population of charged Planck-scale remnants today. In fact, without the introduction of some new physics or novel phenomena, we should expect approximately 50% of BHs to carry a charge at the end of their evaporation; thus, if their evaporation is halted, it is plausible that a substantial portion of the remnant population will be charged [11].

CHAPTER 3

Energy Loss Mechanism and Detection

3.1. The NOvA Far Detector

The NuMI Off-Axis ν_e Appearance (NOvA) experiment is a particle physics experiment designed to detect neutrinos, with the primary goals of observing neutrino oscillations, measuring neutrino interaction cross sections, and searching for evidence of new physics. NOvA utilizes two detectors: a smaller, underground near detector (ND) located at Fermi National Accelerator Laboratory (Fermilab) and a far detector (FD) located at Ash River, MN. The ND is used to characterize the beam and perform cross section measurements, while the FD is used to measure neutrinos at the predicted oscillation maximum and to observe other particles that pass through the detector while the beam is off. The FD is a 14-kiloton liquid scintillator-based detector; a detector of this scale and sensitivity has never been built on the Earth's surface. While most NOvA analyses are concerned with speed-of-light activity in the detectors, the FD offers the ability to search for subluminal exotic particles that would normally be absorbed by the extensive shielding or overburdens (rock and dirt) of other experiments. For example, NOvA has conducted searches for magnetic monopoles using the FD [14].

The FD comprises 344,000 cells crafted from extruded, highly reflective polyvinyl chloride (PVC) filled with liquid scintillator and wavelength-shifting fibers; an illustration of one of these cells is depicted in Figure 3.2. Each cell is 3.9 cm in width, 6.0 cm in depth, and 15.5 m in length. The detector is assembled into modules of 32 cells by joining two 16 cell extrusions together, and the modules are arranged in a pattern of alternating vertical and horizontal orientations, as shown on the left side of Figure 3.1.

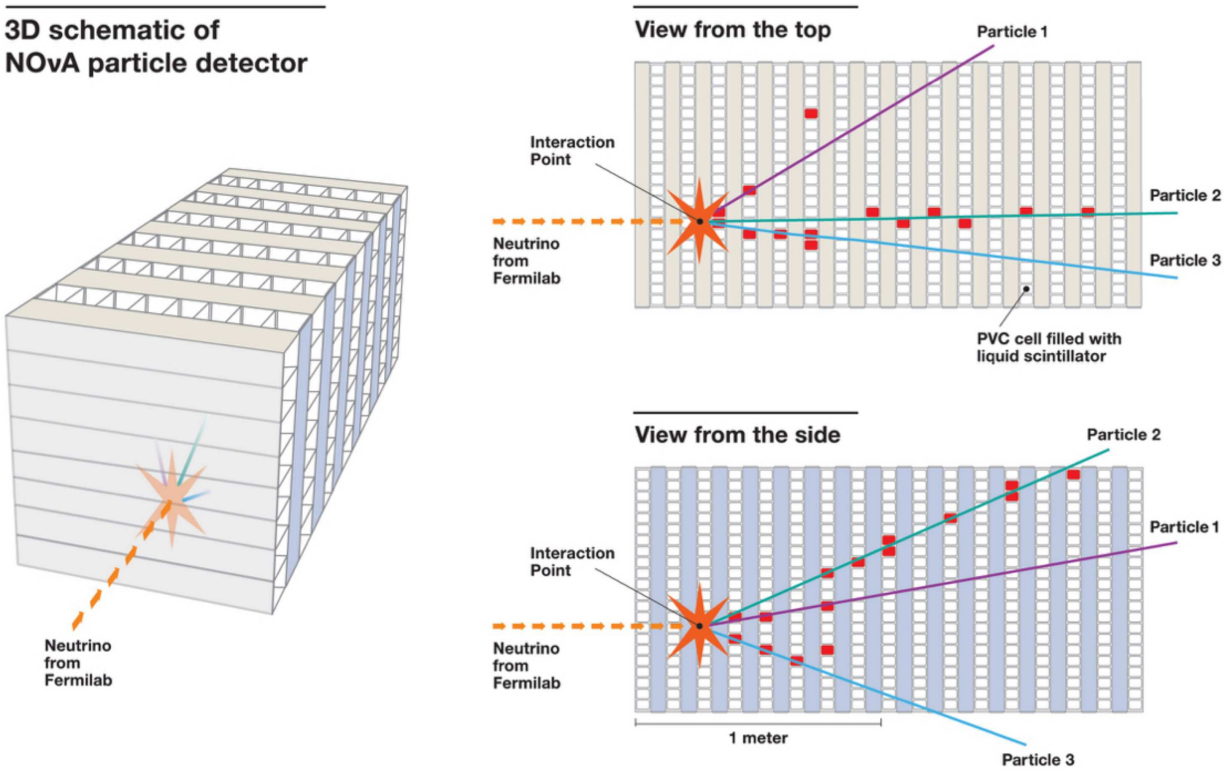

FIGURE 3.1. Schematic of the NOvA detector showing the alternating vertical and horizontal orientations (left). A particle passing through the FD interacts with and excites atoms the scintillator, causing the emission of light (right) [15].

When a charged particle passes through the FD, it imparts visible energy by exciting atoms in the liquid scintillator, causing the emission of light. This emitted light is subsequently collected in the wavelength-shifting fibers, which shift blue light (400–450 nm) from the scintillator into green light (490–550 nm). Some of this green light is then directed onto avalanche photodiodes (APDs); the transition to green light is intentional, as green light is well-matched to the input response of the APDs. The signals from the APDs are then amplified, digitized, and transmitted to the data acquisition system, where both intensity and timing data are extracted and constructed into two- and three-dimensional images[1] based on the geometry of the alternating planes. These resultant images can then be used for

[1]These images are coarse pixel maps of the activity in the detector (see Figure 3.1 for a rough depiction).

particle and event identification. In the context of this analysis, this includes the possibility of identifying charged microscopic BHs moving through the detector.

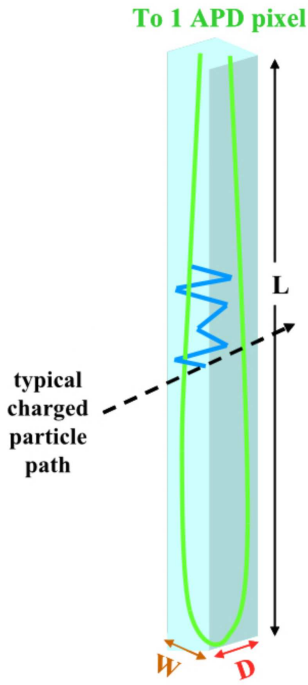

FIGURE 3.2. Illustration of one of the cells that make up the NOvA detector [16]. The wavelength shifting fiber in each cell collects light emitted by the scintillator, from which a signal can be extracted and used for particle analysis.

3.2. Energy Loss Mechanism

Fast moving charged particles travelling through matter primarily lose energy by interacting with the electrons of atoms in the material. This creates a trail of ionizations and excitations along the path of the particle, resulting from energy loss [17]. The Bethe-Bloch equation expresses the mean energy loss per unit distance of a charged particle moving through matter; this is also referred to as the particle's stopping power and is given by

$$-\left\langle \frac{dE}{dx} \right\rangle = Kz^2 \frac{Z}{A} \frac{1}{\beta^2} \left(\frac{1}{2} \ln \frac{2m_e c^2 \beta^2 \gamma^2 T_{max}}{I^2} - \beta^2 \right) \tag{10}$$

where K is a constant, z is the charge of the incident particle, Z and A are the charge and mass number of the material, $\beta = v/c$, m_e is the electron mass, γ is the Lorentz factor, and I is the ionization energy, which is empirically determined; the maximum kinetic energy that can be imparted to an electron in a single collision, T_{max}, is given by

$$T_{max} = \frac{2m_e c^2 \beta^2 \gamma^2}{1 + 2\gamma m_e/M + (m_e/M)^2} \tag{11}$$

where M is the mass of the incident particle [18].

Charged particles can also lose energy by interacting with the nuclei of atoms via elastic scattering; however, for fast moving particles, the magnitude of this loss is generally small compared to electronic interactions [17].

When a microscopic BH interacts with the detector medium, it loses energy via the above mechanisms, transferring energy to atomic electrons and producing ionizations and excitations, and engaging in elastic interactions with nuclei via Coulomb processes; additionally, BHs can lose energy through gravitational interactions [3]. Energy loss by gravitational interactions, per unit length, is given by the following equation

$$\frac{dE}{dx} = \frac{4\pi G^2 M^2 \rho}{v^2} \ln\left(\frac{b_{max}}{b_{min}}\right) \tag{12}$$

where $\rho = m \times n$ is the mass density of the target particles of mass m, n is the number density of the target particles, and b_{max} and b_{min} are the maximum and minimum impact parameters respectively; the term $\ln\left(\frac{b_{max}}{b_{min}}\right)$ changes weakly across a wide range of impact parameters, taking on a value between 10 and 30 [3].

For a microscopic BH of mass 10^{-5} g and velocity 250 km/s, Equation 12 evaluates to $\sim 10^{-21}$ keV cm^2/g; thus, gravitational energy loss can be neglected relative to electronic and

nuclear energy losses. Furthermore, at very low energies, the interaction of the microscopic BH with nuclei dominates over the contribution from the interaction with electrons [3].

These BHs are expected to have velocities in the range of 250-1250 km/s [3], making them highly non-relativistic ($\beta \sim 10^{-4}$ or 10^{-3}). At these low energies, the electronic stopping power is given by

$$S_{el}(E) = \frac{1}{\rho} \times \left(\frac{dE}{dx}\right)_{el} = 2.307 \times 10^9 \times \frac{Z^{7/6} Z_{det}}{\left(Z^{2/3} + Z_{det}^{2/3}\right)^{3/2}} \times \frac{1}{A_{det}} \times \left(\frac{E}{A}\right)^{1/2} \tag{13}$$

where Z_{det} is the charge of the detector medium, Z is the effective charge of the BH, A_{det} and A are the mass numbers of the detector medium and the BH respectively, and E is the kinetic energy of the BH.

The nuclear stopping power is given by

$$S_{nucl}(E) = \frac{1}{\rho} \times \left(\frac{dE}{dx}\right)_{nucl} = 5.097 \times 10^9 \times \frac{Z Z_{det}}{(A + A_{det}) \left(Z^{2/3} + Z_{det}^{2/3}\right)^{1/2}} \times \frac{A}{A_{det}} \times S_n(\epsilon) \tag{14}$$

where $S_n(\epsilon)$, the reduced nuclear stopping cross section, is given by

$$S_n(\epsilon) = \frac{1}{2} \frac{\log(1+\epsilon)}{\epsilon + 0.10718\epsilon^{0.37544}} \tag{15}$$

and ϵ, the reduced energy, is defined as

$$\epsilon = \frac{32.53 A_{det}}{A + A_{det}} \times \frac{E}{Z Z_{det} \left(Z^{2/3} + Z_{det}^{2/3}\right)^{1/2}} \tag{16}$$

At these low energies, nuclear energy losses are primarily due to elastic collisions between the BH and the nuclei in the target material. The electronic and nuclear stopping powers in Equations 13 and 14 are expressed in units of eV·cm^2/g [3].

Lehmann suggests that the upper limit of energy transfer from a small, charged BH to a recoiling electron is lower than typical ionization energies, so direct ionization via electronic interactions is not likely to be efficient. However, the maximum energy transfer during a recoil event involving a nucleus is significantly greater than that in electronic recoils; thus, we indeed expect interactions between the BH and nuclei to dominate in a typical detector [11]. Although ionization and scintillation are most efficiently produced by electronic interactions, nuclear stopping can also generate these signals because some of the recoil energy of the nucleus can be transferred to bound electrons. Therefore, as a BH moves through a detector, shedding energy through Coulomb interactions with the target electrons and nuclei, the transferred energy can manifest as detectable heat, ionization, or scintillation [11].

The interactions between a small, charged BH and matter closely resemble those of slowly moving, heavy ions. A BH with a mass on the order of the Planck scale will experience minimal deceleration as it traverses through the detector medium; even in the presence of a strong electromagnetic field, deflection is also negligible, resulting in the BH depositing energy along a very straight track [11]. The trajectories of these microscopic BHs will therefore traverse the entire active medium, in any direction, producing uniform ionization and scintillation for the entirety of their path [3]. It is possible to discriminate between the signals (ionization and scintillation) produced by microscopic BHs relative to other heavy ions or other particles, namely cosmic ray muons. Muons are the only appreciable background to

consider, as they also deposit energy along straight tracks, as opposed to showers produced by other particle interactions.

Depending on the electric charge, microscopic BHs can capture protons or electrons to form neutral "atoms". A charged collapsed object moving through matter at a velocity less than a few thousand km/s would tend to capture electrons (if $Z > 0$) to form an electronic atom, or protons (if $Z < 0$) to form a protonic atom. In the former case, the radius of the atom would be similar to that of an ordinary atom, but in the latter case it would be 1800 times smaller [13].

However, following the assumptions of Lazanu [3], we will suppose that as a microscopic BH passes through the detector, it does not change its electrical charge through loss or capture of electrons or protons, for a positively or negatively charged BH, respectively. The effective charge of the BH is given by

$$q \cong Z\left(1 - e^{-v/Z^{2/3}v_{Bohr}}\right) \tag{17}$$

where Z is the bare charge of the BH, v is the BH's velocity, and v_{Bohr} is Bohr's velocity, which has a value of 2.18×10^6 m/s. For a BH with a mass of 10^{-5} g and a velocity of 250 km/s, the relative variation in its velocity over the 60 m length of the detector is minimal, only about 10^{-6}% [3]. Thus, we can treat the effective charge as remaining constant as the BH traverses the detector.

CHAPTER 4

Analysis

4.1. Energy Loss Calculation

This chapter describes the current state of the BH remnant analysis and the steps that have been accomplished thus far to determine the feasibility of performing a search for these microscopic BHs using the NOvA FD. The goal of this stage of the analysis was to develop code using Python to model the BHs passing through the FD to determine if microscopic BHs would generate a signal sufficiently different from the primary expected background, cosmic ray muons.

The first step in this analysis was to create a program to simulate microscopic BHs passing through the NOvA FD. The coordinate system and orientation used to define the detector is shown in Figure 4.1 below. Planck mass BHs were generated and simulated traversing

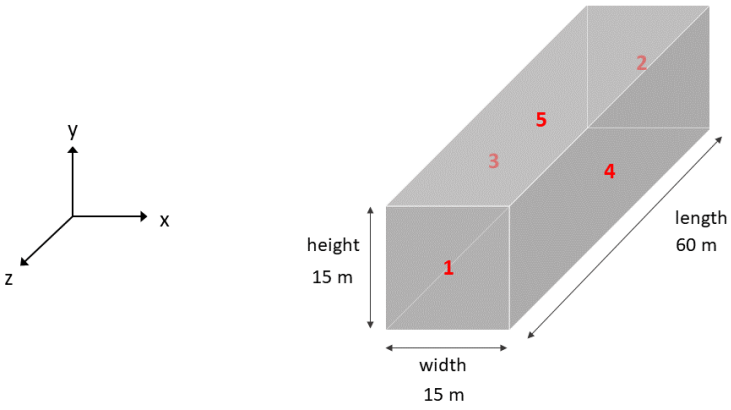

Figure 4.1. Schematic of the coordinate system and detector orientation used in the analysis. Sides are labeled 1-5 for clarity. The detector is oriented such that side 1 faces SSE toward Fermilab.

through the detector at specified initial velocities of 250, 500, 750, 1000, and 1250 km/s. The BHs were generated such that they traverse the detector on a set trajectory, namely moving

in a straight path through the center of each of the 5 faces of the detector; BHs entering the detector from below, through the bottom face, were not examined. While several different trajectories through the detector were investigated, only the trajectories through the 60 m length (entering through side 1) were presented in order to make meaningful comparisons between BHs, and muons, with particular properties; Figure 4.2 shows a pseudo-event display depicting this trajectory.

Effective BH charges were mapped to bare, unscreened charges of 1, 5, 10, and 20. The kinetic energy, as well as the electronic and nuclear stopping power (Equations 13 and 14), of each BH was calculated as it passed through the detector; the FD is mostly made up of carbon, so the charge and mass number of carbon were used for Z_{det} and A_{det} respectively. These values were recorded at incremental steps, with a step size of 1 cm used for all cases. Plots of the stopping power as a function of position were generated for each simulated BH, as well as histograms of the stopping power (Figures 4.3 and 4.4, respectively).

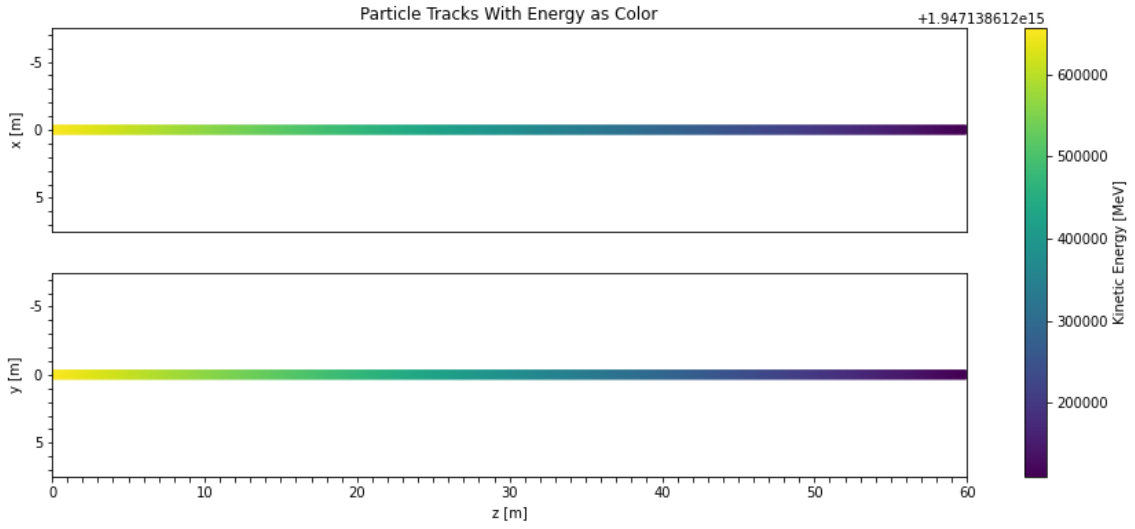

FIGURE 4.2. Pseudo-event display showing the kinetic energy for a simulated microscopic BH passing through the length of the detector after entering through the center of side 1, with a charge of 1 and a velocity of 250 km/s.

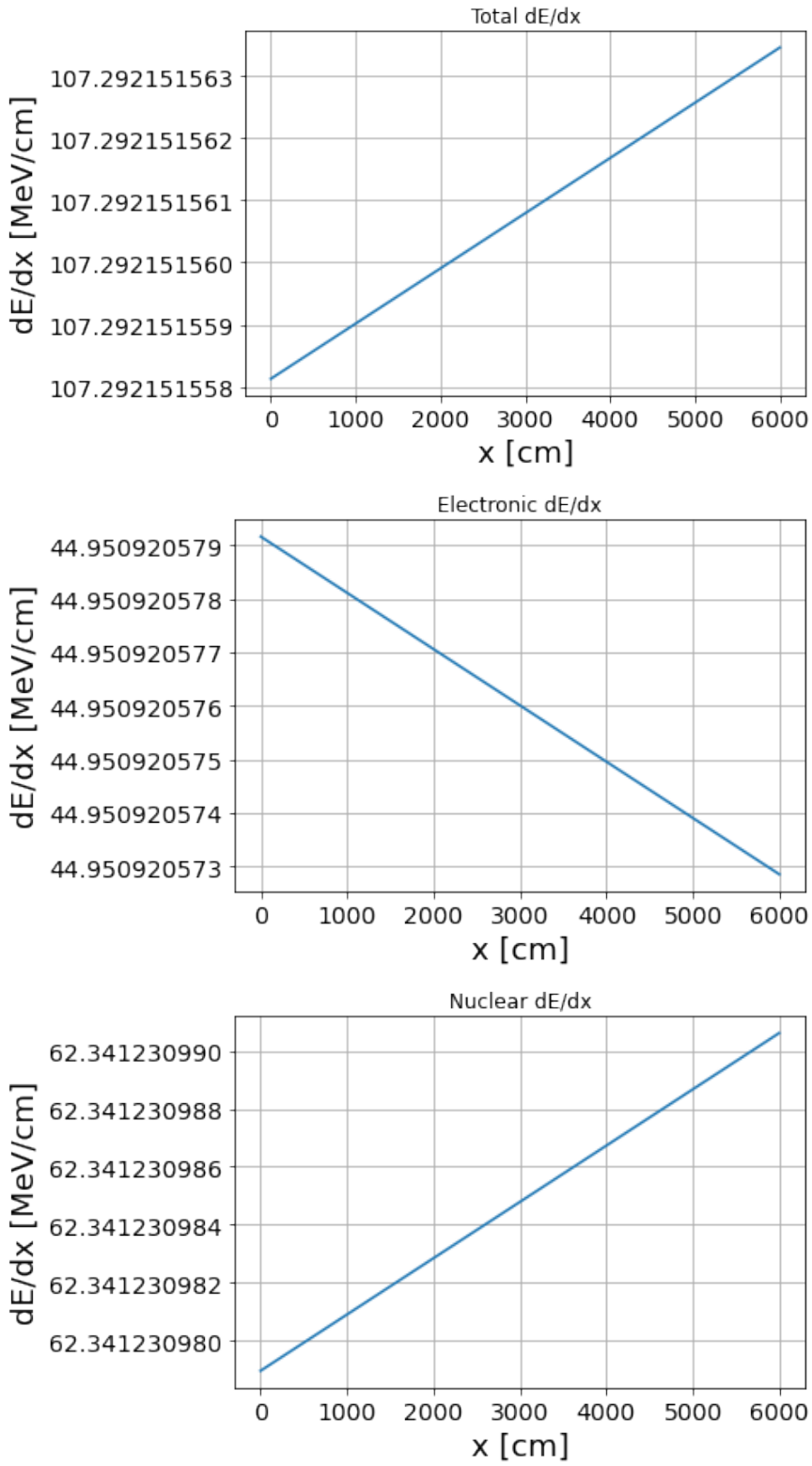

FIGURE 4.3. Plots of the total, electronic, and nuclear stopping power as a function of position for a microscopic BH passing through side 1 of the detector, with a charge of 1 and a velocity of 250 km/s.

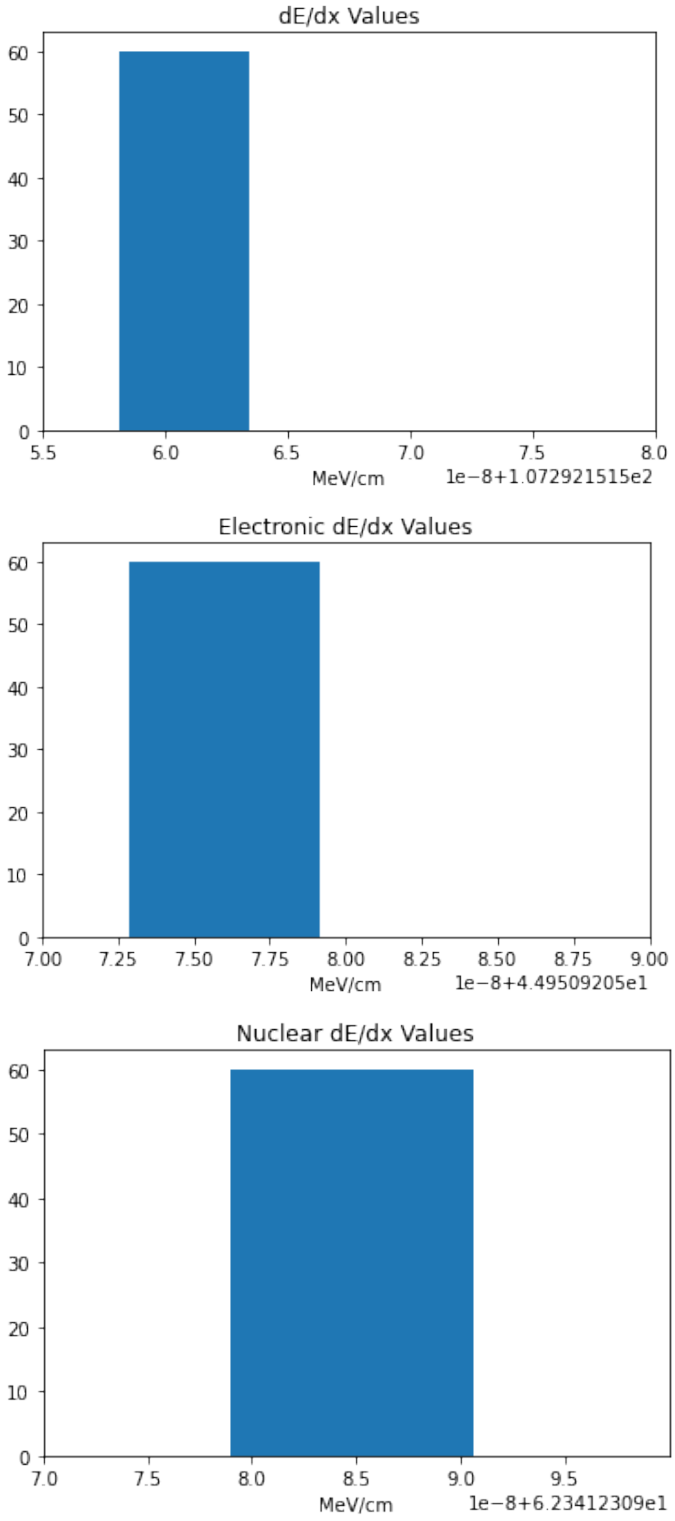

FIGURE 4.4. Histograms of the total, electronic, and nuclear stopping power for a simulated microscopic BH passing through side 1 of the detector, with a charge of 1 and a velocity of 250 km/s.

The change in kinetic energy for BHs with charge and velocity parameters within the stated range is shown in Figure 4.5. Table 4.1 summarizes these values, as well as the mean electronic and nuclear energy losses, and corresponding standard deviations.

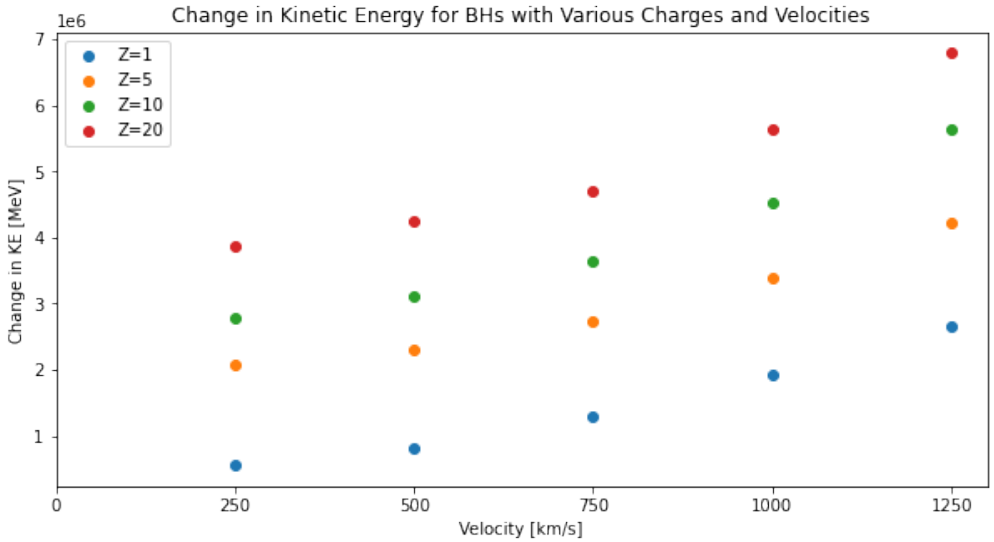

FIGURE 4.5. Plot of the change in kinetic energy for various BH charges and velocities; these BHs were again generated to pass through the length of the detector after entering through the center of side 1.

The effective charge mapping from Lazanu [3] that was used in this analysis corresponded to BHs traversing through liquid argon (LAr). In general, the effective charge of a slow moving, heavy ion depends on the medium it is travelling through. The NOvA FD is mostly composed of carbon, so the effective charge of the BH would be inherently different in this material compared to LAr. This material dependence proved to be too complicated to be implemented properly at this stage of the analysis, so further study will be required to ensure accurate treatment of the effective charge.

As an alternative, the simulation was carried out again with the effective charge mapping varied by $\pm$ 20%. Table 4.2 shows the change in kinetic energy and mean electronic and nuclear energy losses, with the adjusted effective charge mappings implemented.

TABLE 4.1. Summary of BH simulation data with the change in kinetic energy, mean electronic and nuclear energy losses, and corresponding standard deviations for different BH bare charge and velocity values.

ΔKE (MeV)	$\left(\overline{dE/dx}\right)_{elec}$ (MeV/cm)	σ_{elec} (MeV/cm)	$\left(\overline{dE/dx}\right)_{nucl}$ (MeV/cm)	σ_{nucl} (MeV/cm)	Charge (Units of e)	Velocity (km/s)
547,265.5	44.951	$\pm$ 1.824$\times10^{-9}$	62.341	$\pm$ 3.365$\times10^{-9}$	1	250
2,067,971.5	112.459	$\pm$ 3.478$\times10^{-8}$	292.738	$\pm$ 4.825$\times10^{-8}$	5	250
2,770,924.5	136.189	$\pm$ 5.391$\times10^{-8}$	406.706	$\pm$ 6.799$\times10^{-8}$	10	250
3,876,463.75	168.988	$\pm$ 9.014$\times10^{-8}$	590.475	$\pm$ 1.176$\times10^{-7}$	20	250
798,882.0	119.005	$\pm$ 3.391$\times10^{-9}$	37.94	$\pm$ 7.58$\times10^{-10}$	1	500
2,302,289.0	272.379	$\pm$ 1.582$\times10^{-8}$	178.03	$\pm$ 5.645$\times10^{-9}$	5	500
3,113,752.0	337.976	$\pm$ 2.622$\times10^{-8}$	272.306	$\pm$ 1.056$\times10^{-8}$	10	500
4,252,315.0	416.81	$\pm$ 4.428$\times10^{-8}$	416.099	$\pm$ 1.815$\times10^{-8}$	20	500
1,283,242.0	220.518	$\pm$ 4.369$\times10^{-9}$	30.171	$\pm$ 2.83$\times10^{-10}$	1	750
2,730,038.0	425.629	$\pm$ 1.081$\times10^{-8}$	109.152	$\pm$ 2.964$\times10^{-9}$	5	750
3,648,436.0	537.802	$\pm$ 1.909$\times10^{-8}$	177.374	$\pm$ 5.576$\times10^{-9}$	10	750
4,705,224.0	652.81	$\pm$ 2.857$\times10^{-8}$	269.054	$\pm$ 1.141$\times10^{-8}$	20	750
1,912,284.0	347.919	$\pm$ 5.011$\times10^{-9}$	26.498	$\pm$ 2.1$\times10^{-10}$	1	1,000
3,396,820.0	589.885	$\pm$ 1.076$\times10^{-8}$	76.892	$\pm$ 1.456$\times10^{-9}$	5	1,000
4,529,092.0	757.01	$\pm$ 1.925$\times10^{-8}$	131.228	$\pm$ 2.845$\times10^{-9}$	10	1,000
5,636,204.0	906.27	$\pm$ 2.736$\times10^{-8}$	196.066	$\pm$ 5.64$\times10^{-9}$	20	1,000
2,667,128.0	499.768	$\pm$ 6.786$\times10^{-9}$	24.405	$\pm$ 1.17$\times10^{-10}$	1	1,250
4,227,152.0	764.887	$\pm$ 1.131$\times10^{-8}$	58.854	$\pm$ 8.77$\times10^{-10}$	5	1,250
5,636,200.0	994.802	$\pm$ 2.062$\times10^{-8}$	104.75	$\pm$ 1.748$\times10^{-9}$	10	1,250
6,793,640.0	1,176.546	$\pm$ 2.804$\times10^{-8}$	153.891	$\pm$ 3.339$\times10^{-9}$	20	1,250
[1] 13,076.46	2.561	$\pm$ 0.148	–	–	1	299,785.120

[1]This row corresponds to a 15 GeV muon; at this energy, electronic losses are dominant and nuclear losses are negligible.

TABLE 4.2. Summary of adjusted BH simulation data with the change in kinetic energy and mean electronic and nuclear energy losses for different BH bare charge and velocity values.

[2] **Effective Charge Decreased by 20%**			[3] **Effective Charge Increased by 20%**				
ΔKE (MeV)	$\left(\overline{dE/dx}\right)_{elec}$ (MeV/cm)	$\left(\overline{dE/dx}\right)_{nucl}$ (MeV/cm)	ΔKE (MeV)	$\left(\overline{dE/dx}\right)_{elec}$ (MeV/cm)	$\left(\overline{dE/dx}\right)_{nucl}$ (MeV/cm)	[4] Charge (Units of e)	Velocity (km/s)
404,158.75	35.961	43.065	702,953.0	53.748	83.981	1	250
1,536,432.0	92.227	208.685	2,627,817.75	131.572	383.257	5	250
2,067,971.5	112.459	292.738	3,503,757.0	158.396	527.873	10	250
2,915,603.75	140.746	430.441	4,864,057.5	195.109	757.763	20	250
622,750.0	95.81	25.744	987,594.0	141.497	51.934	1	500
1,773,895.0	224.918	123.165	2,836,974.0	316.792	239.436	5	500
2,409,226.0	281.492	189.819	3,849,729.0	390.217	363.706	10	500
3,283,593.0	350.384	292.664	5,252,490.0	477.49	551.241	20	500
1,019,046.0	178.508	20.339	1,547,440.0	260.938	41.543	1	750
2,176,482.0	352.012	74.489	3,283,594.0	494.371	148.626	5	750
2,918,750.0	449.051	121.801	4,390,704.0	619.609	240.155	10	750
3,761,664.0	549.887	185.923	5,661,366.0	746.578	362.2	20	750
1,534,860.0	282.994	17.799	2,289,708.0	409.964	36.6	1	1,000
2,767,780.0	488.592	52.097	4,025,860.0	684.276	105.385	5	1,000
3,698,760.0	633.587	89.405	5,359,428.0	870.415	178.95	10	1,000
4,579,416.0	764.863	134.233	6,642,668.0	1,034.772	266.181	20	1,000
2,163,904.0	408.261	16.356	3,170,368.0	586.689	33.777	1	1,250
3,421,984.0	634.463	39.695	4,931,680.0	886.183	80.992	5	1,250
4,629,736.0	834.482	71.015	6,542,024.0	1,141.668	143.48	10	1,250
5,636,200.0	994.802	104.75	7,900,752.0	1,341.307	210.023	20	1,250

[2]The values in these columns correspond to a 20% decrease in the effective charge mapping from Lazanu [3].
[3]These values correspond to a 20% increase in the effective charge mapping.
[4]Here, "charge" refers to the bare charge of the BH before conversion to an effective charge.

Cosmic muons were also examined in a similar manner, as they are predicted to be the only appreciable background. Muons with kinetic energy of 15 GeV and thus corresponding velocity of approximately 0.99c were generated such that they traversed through the full 60 m length of the detector.

The kinetic energy and stopping power of each muon was similarly tracked through the detector, implementing the Bethe-Bloch formula (Equation 10) for stopping power for the muons, as their velocity was above the Bethe-Bloch threshold; examples of these plots are shown in Figures 4.6 and 4.7 below. A histogram of the stopping power was also generated for each simulated muon (Figure 4.8).

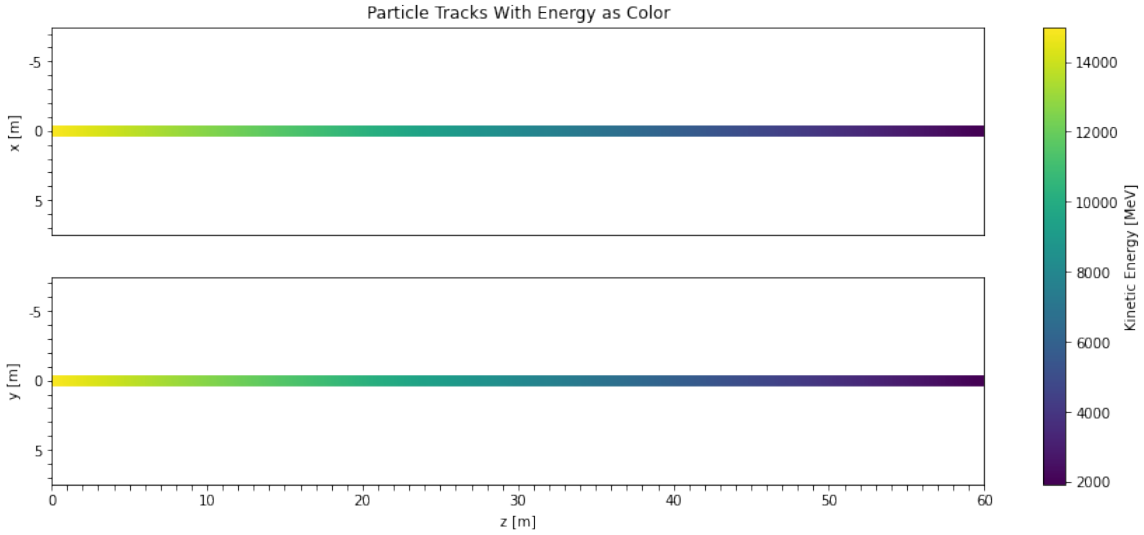

FIGURE 4.6. Plot of kinetic energy for a simulated muon passing through side 1 of the detector, with a kinetic energy of 15 GeV.

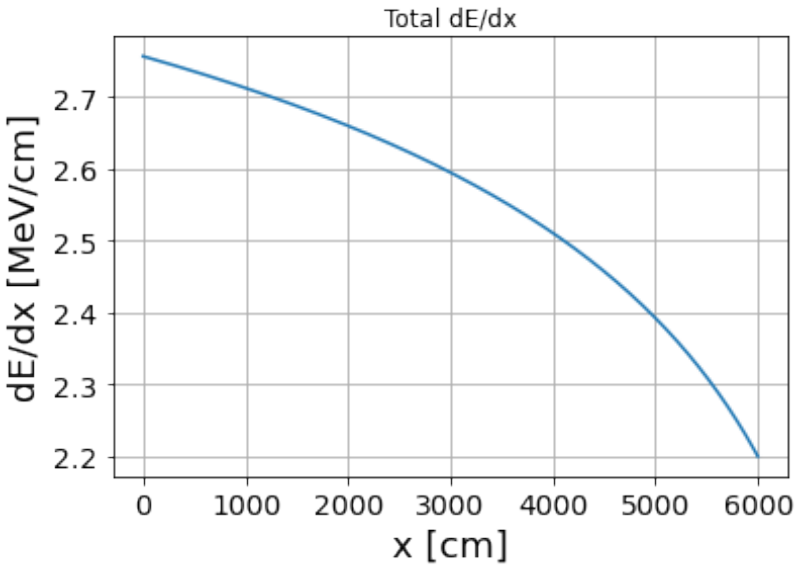

FIGURE 4.7. Plot of the total stopping power as a function of position for a muon passing through side 1 of the detector, with a kinetic energy of 15 GeV.

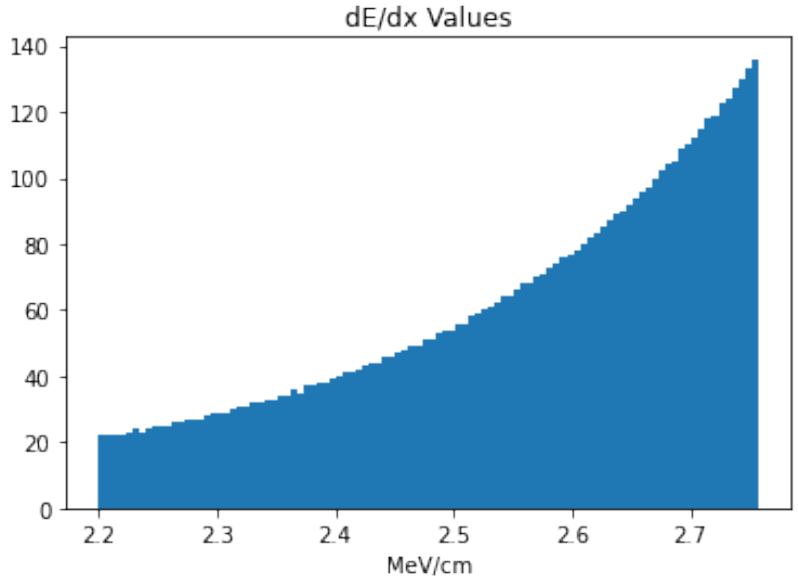

FIGURE 4.8. Histogram of total stopping power for a simulated muon passing through side 1 of the detector, with a kinetic energy of 15 GeV.

This process was again repeated for protons with a velocity of 0.5c. At this velocity, protons lose energy in a similar manner to BHs, primarily through nuclear interactions; thus, a comparison could be made since we already understand how signals induced by

protons appear in the detector. A plot of the total stopping power as a function of position is shown in Figure 4.9 below, and a histogram of the stopping power is shown in Figure 4.10.

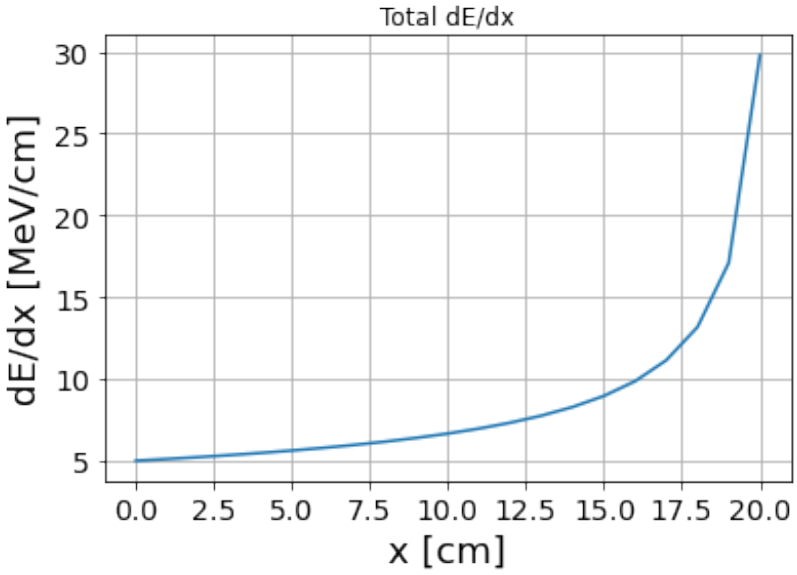

FIGURE 4.9. Plot of the total stopping power as a function of position for a proton passing through side 1 of the detector, with a velocity of 0.5c.

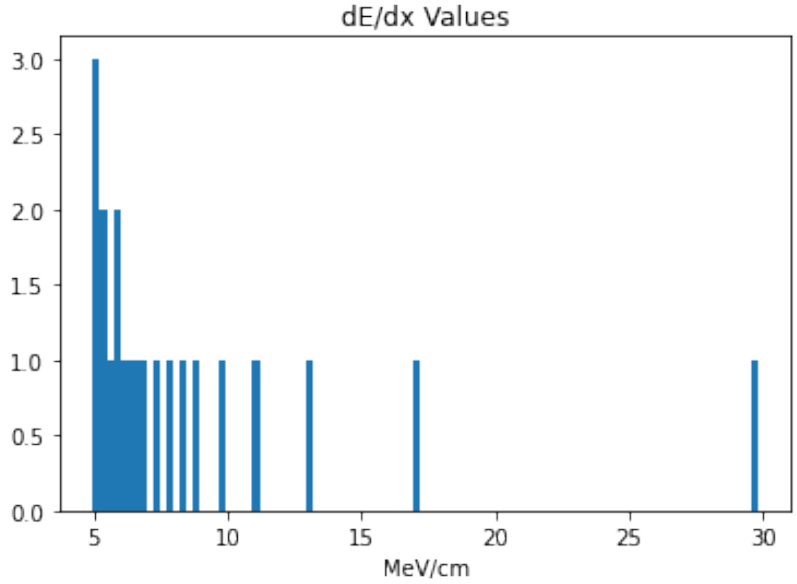

FIGURE 4.10. Histogram of total stopping power for a simulated proton passing through side 1 of the detector, with a velocity of 0.5c.

4.2. Charge Distribution

Charge values were extrapolated from Page [12] to create a plot of the relative probability distribution for the charge of a microscopic BH. Page gave a predicted probability distribution for the charge Z of a BH; this was scaled to a relative probability distribution with a maximum value of 1, as shown in Figure 4.11 below.

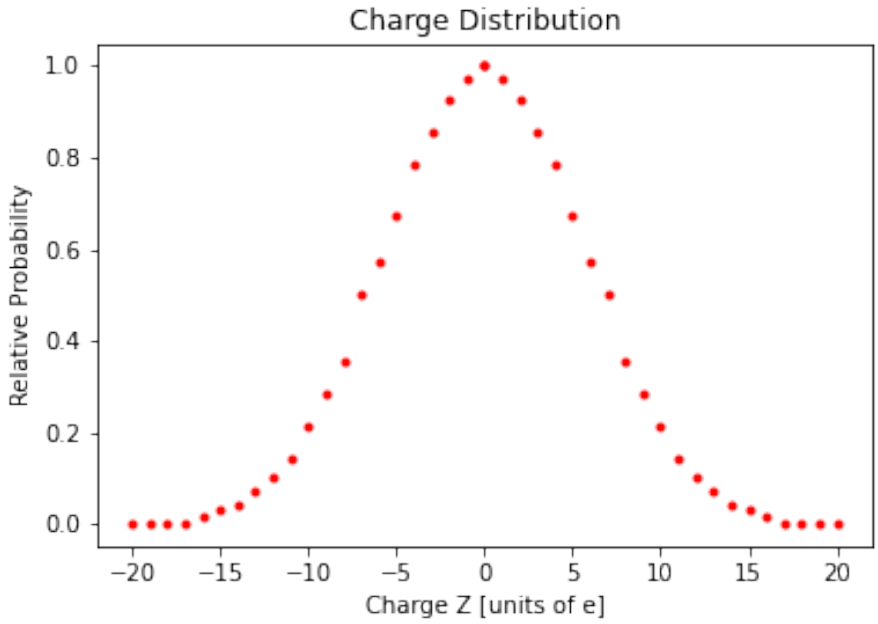

Figure 4.11. Relative probability for the charge Z of a microscopic BH.

CHAPTER 5

Results and Future Directions

5.1. Analysis Results

From Figure 4.4, the total energy loss of the BH was approximately 107.29 MeV/cm, with 44.95 MeV/cm corresponding to electronic energy losses and 62.34 MeV/cm corresponding to nuclear losses. Comparing this with Figures 4.8 and 4.10, the total energy loss was significantly higher for the microscopic BH compared to the muon and proton. On average, the nuclear losses of the BH were more than an order of magnitude greater than the proton.

Electronic interactions are more efficient at producing ionization and scintillation compared to nuclear interactions. For protons at the energy scale used in this analysis, nuclear interactions dominate, so observing them using the NOvA FD is difficult because many detector nuclei collectively absorb the energy loss. This results in a limited number of scattered particles with sufficient energy for detection. Thus, BH nuclear energy losses of this magnitude will lead to incomplete tracks and a sporadic visible signal along the path of the BH. Further study will be required to determine if it is possible to detect BHs using the NOvA FD and over what range of parameter space.

A rough estimate of the range of each object was also calculated, assuming an infinitely long detector. The BH travelled significantly farther before stopping, with a predicted range of 3×10^8 km; the predicted range for the muon was 72 m, and the proton travelled 0.21 m before stopping.

5.2. Future Directions

The goal of this analysis was to explore the feasibility of detecting microscopic BHs with the NOvA FD. The analysis was completed using a program that has served as an approximation to the NOvA software. Without further study employing the full NOvA simulation chain, it remains uncertain whether detecting microscopic BHs with the NOvA FD is possible; if such detection is indeed possible, the range of BH properties over which it can be achieved is also unclear. Thus, a crucial next step will be to implement this analysis into the NOvA software. This step will be carried out over the next several months.

Particle detectors can achieve different levels of accuracy in particle detection, depending on their specific design. The timing resolution of a detector determines how well events happening in quick succession can be distinguished from one another [19]. For example, this can be used to determine the time that a particle, such as a microscopic BH, passes into and out of the detector, as well as the cells within it; the direction the particle is moving can also be determined. This is an essential tool for event identification and reconstruction. The timing resolution is influenced by the properties of the detector, such as the detector material, the scintillation counter, and the type of light guide being used [19]. The channel-to-channel timing resolution of the NOvA FD is about 20 ns; however, other particle detectors may achieve even better timing resolutions, such as the Deep Underground Neutrino Experiment (DUNE).

In addition to timing resolution, the spatial and energy resolutions of a detector also influence particle detection. The spatial resolution of a detector refers to its accuracy in reporting the precise location of a particle interaction, specifically the vertex of the interaction within the detector; it also refers to the ability of the detector to differentiate the signals

it receives due to two distinct particles passing in close proximity to one another [19]. The energy resolution determines how well energy can be measured in the detector. Compared to NOvA, DUNE also has better spatial and energy resolutions. For this reason, an additional study will be carried out to assess the feasibility of performing the analysis on DUNE.

CHAPTER 6

Conclusion

This thesis assessed the practicality of directly detecting microscopic BHs with current particle detectors, namely NOvA. The formation and stability of microscopic BHs was summarized, with an emphasis on the generalized uncertainty principle (GUP) as a way for these objects to exist and survive from the early universe. Their properties were outlined, including their mass, expected velocity range, and predicted charge distribution. The energy loss mechanism of microscopic BHs was described, and an analysis was carried out to simulate the BHs passing through the NOvA FD. This analysis served as a relatively simple approximation to the NOvA software, and the goal of this stage was to determine if microscopic BHs would generate signals distinguishable from other particles, such as cosmic ray muons and protons.

While the preliminary results showed significant differences between the signals produced by microscopic BHs and those produced by muons and protons, there is not yet conclusive evidence supporting the feasibility of conducting this analysis with the NOvA experiment. The nuclear energy losses of the BHs calculated in this analysis would lead to a sporadic visible signal in the NOvA FD, so further study using the NOvA software is required to make a final determination of the ability to detect microscopic BHs with the NOvA FD. Future steps will also seek to assess the possibility of implementing this analysis into other experiments, namely DUNE.

In addition to providing direct evidence of the existence of dark matter, detection of these microscopic BHs would confirm the primordial BH paradigm, offering insight into the conditions of the early universe [11]. The presence of a substantial number of these objects

would allow for the direct study of gravity in the quantum regime. Even the detection of a single microscopic BH would demonstrate that they do not evaporate completely, but leave behind a remnant, which would have substantial implications for our understanding of BH physics, the behavior of gravity at the quantum level, and the nature of dark matter [11].

Bibliography

[1] R. J. Adler, P. Chen, and D. I. Santiago, "The generalized uncertainty principle and black hole remnants," *General Relativity and Gravitation*, vol. 33, pp. 2101–2108, December 2001.

[2] P. Chen, "Inflation induced planck-size black hole remnants as dark matter," *New Astronomy Reviews*, vol. 49, pp. 233–239, May 2005.

[3] I. Lazanu, S. Lazanu, and M. Pârvu, "About detecting very low mass black holes in LAr detectors," *Journal of Cosmology and Astroparticle Physics*, vol. 10, p. 046, October 2020.

[4] P. H. Frampton, M. Kawasaki, F. Takahashi, and T. T. Yanagida, "Primordial black holes as all dark matter," *Journal of Cosmology and Astroparticle Physics*, vol. 2010, April 2010.

[5] A. Kashlinsky, "LIGO gravitational wave detection, primordial black holes, and the near-ir cosmic infrared background anisotropies," *The Astrophysical Journal*, vol. 823, May 2016.

[6] S. Bird, A. Albert, W. Dawson, Y. Ali-Haïmoud, A. Coogan, A. Drlica-Wagner, Q. Feng, D. Inman, K. Inomata, E. Kovetz, *et al.*, "Snowmass2021 cosmic frontier white paper: Primordial black hole dark matter," *Physics of the Dark Universe*, vol. 41, August 2023.

[7] S. Hawking, "Black hole explosions?," *Nature*, vol. 248, pp. 30–31, March 1974.

[8] S. Hawking, "Particle creation by black holes," *Communications in Mathematical Physics*, vol. 43, pp. 199–220, August 1975.

[9] C. W. Misner, K. S. Thorne, and J. A. Wheeler, *Gravitation*. W.H. Freeman and Company, 1973.

[10] A. D. Helfer, "Do black holes radiate?," *Reports on Progress in Physics*, vol. 66, pp. 943–1008, May 2003.

[11] B. V. Lehmann, C. Johnson, S. Profumo, and T. Schwemberger, "Direct detection of primordial black hole relics as dark matter," *Journal of Cosmology and Astroparticle Physics*, vol. 2019, p. 046, October 2019.

[12] D. Page, "Particle emission rates from a black hole. III. Charged leptons from a nonrotating hole," *Physical Review D*, vol. 16, pp. 2402–2411, October 1977.

[13] S. Hawking, "Gravitationally collapsed objects of very low mass," *Monthly Notices of the Royal Astronomical Society*, vol. 152, pp. 75–78, April 1971.

[14] A. Acero *et al.*, "Search for slow magnetic monopoles with the NOvA detector on the surface," *Physical Review D*, vol. 103, January 2021.

[15] E. Catano-Mur, "Recent results from NOvA," 2022.

[16] B. Behera, "Tracking detector performance and data quality in the NOvA experiment," 2017.

[17] E. A. Uehling, "Penetration of heavy charged particles in matter," *Annual review of nuclear science*, vol. 4, no. 1, pp. 315–350, 1954.

[18] R. L. Workman *et al.*, "Review of particle physics," *PTEP*, 2022.

[19] W. Frass and R. Walczak, *Particle detectors*. Oxford Physics, 2009.